



Soft Matter

Customized Metallodielectric Colloids and their Behavior in Dielectrophoretic Fields

Journal:	<i>Soft Matter</i>
Manuscript ID	SM-ART-08-2022-001099.R1
Article Type:	Paper
Date Submitted by the Author:	22-Sep-2022
Complete List of Authors:	Dong, Fangyuan; New York University, Molecular Design Munkaila, Samira; NEW YORK UNIVERSITY, NEW YORK UNIVERSITY Grebe, Veronica; New York University, Molecular Design Institute and Weck, Marcus; New York University, Molecular Design Ward, Michael; New York University, Chemistry

SCHOLARONE™
Manuscripts

ARTICLE

Customized Metallodielectric Colloids and their Behavior in Dielectrophoretic Fields

Fangyuan Dong, Samira Munkaila, Veronica Grebe, Marcus Weck,* and Michael D. Ward*

Received 00th January 20xx,
Accepted 00th January 20xx

DOI: 10.1039/x0xx00000x

A synthetic strategy for fabricating colloidal particles with spatially segregated amine-functionalized lobes enables regioselective coating with gold to afford metallodielectric particles with a variety of shapes and lobe sizes. This approach can produce either dissymmetric dumbbell-shaped two-lobed Au-TPM particles (**Au-T**) or dissymmetric or symmetric three-lobed particles with gold coating on one (**Au-T-T** and **T-Au-T**) or two lobes (**Au-T-Au**). Dielectrophoretic (DEP) forces exerted by an AC field confined between two opposing electrodes generate aggregates ranging from 1D chains to 2D close-packed lattices, depending on the particle shape and lobe arrangement. The aggregate structures reflect the lowest energy configurations resulting from the induced dipole moments created in particle lobes within the confined electric field.

1 Introduction

Colloidal particles can be programmed to assemble into ordered superstructures, including colloidal crystals.¹ The complexity and utility of colloidal crystals, however, remain limited by the ability to synthesize structurally diverse and intricate anisotropic building blocks as well as challenges in controlling their assembly.^{2, 3} Unlike isotropic colloidal particles, anisotropic particles can assemble into structures with controlled long-range order, either through prescribed valency or spatial asymmetry,⁴⁻⁷ which is essential for achieving properties related to solar cells, computer chips, metamaterials (e.g., photonic crystals), biosensors, and micromirrors.⁸⁻¹¹ Anisotropic colloids can be classified generally according to shape anisotropy and compositional surface anisotropy.¹² Colloidal particles with shape anisotropy have been fabricated by photolithography,¹³ mechanical deformation,¹⁴ or seeded growth.¹⁵ Surface anisotropy has been achieved through regioselective modification of a particle surface, as exemplified by patchy particles and Janus particles, using methods such as microcontact printing,¹⁶ DNA coating,¹⁷ and metal deposition.¹⁸ Application of external forces, such as electric or magnetic fields, can regulate particle assembly into complex, even ordered, structures by introducing directional interparticle interactions.^{12, 19} Electrophoresis and dielectrophoresis (DEP) have been used for this purpose because of their experimental simplicity.^{20, 21} Directional interactions between particles result from the introduction of asymmetric pair potentials and local/global potential gradients created by the external fields.^{12, 21} The manipulation of particles in electric fields can be achieved at various length scales ranging from nano- to mesoscale

for both charged and neutral particles.^{22, 23} DEP forces arise from a nonuniform electric field on dielectric colloidal particles, which can result in directional particle motion parallel to the electric field as well as particle-particle interactions caused by induced dipoles.²⁴ DEP forces can be adjusted precisely by tuning field parameters such as magnitude, frequency, wave shape, wave symmetry, and phase.¹⁸ These advantages make DEP one of the most effective and robust method to assemble colloids into 1D chains, 2D crystal lattices, or 3D bundles with various symmetries.²⁵⁻²⁷ For example, our laboratory demonstrated that three-patch particles can be directed to form helical coiled chains in a DEP cell.²⁵ Nonetheless, much remains to be learned of the effects of shape and surface anisotropy on lattice structure.

Recent studies have revealed anisotropic assembly of metallodielectric patchy particles in DEP fields,²⁸ resulting in staggered chains, either parallel or perpendicular to the surface of the DEP cell, as well as open-brick lattices.²⁸ Percolated networks have been observed for metallodielectric patchy particles under a high frequency AC electric field.²⁹ The current synthetic routes for the fabrication of these particles, however, precludes systematic adjustment of particle shape or requires encapsulation of colloidal particle clusters, the latter producing a mixture of different particle symmetries.

Our laboratory recently reported a facile sequential seeded growth approach to fabricating multicomponent particles with tunable anisotropic shapes and components, enabling regioselective chemical anisotropy on the particle surfaces.^{15, 30} Herein, we report a synthetic methodology that introduces surface anisotropy to shape-anisotropic particles through site-specific coating with gold, resulting in multi-component particles with low dispersity and facile tunability. Under the influence of DEP fields, these new particles can be assembled into 1D and 2D structures (Figure 1).

Molecular Design Institute, Department of Chemistry, New York University, New York, New York 10003, USA.

Electronic Supplementary Information (ESI) available: Experimental details, details on the DEP device, and additional figures. See DOI: 10.1039/x0xx00000x

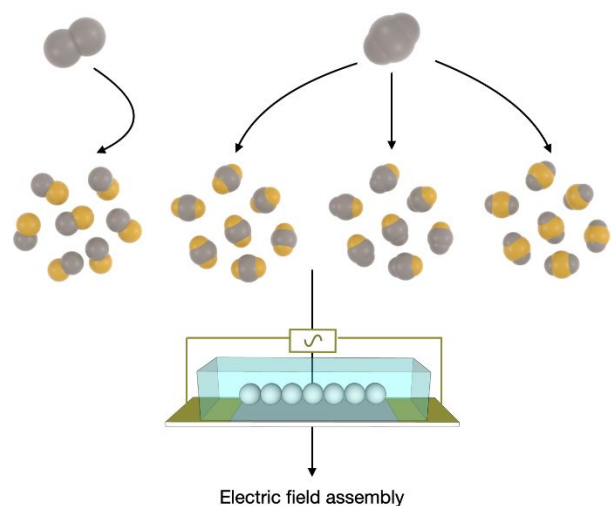


Fig. 1 (top) Schematic representation of various anisotropic metalodielectric patchy particles with gold-coated lobes. (bottom) Schematic representation of particle assembly under the influence of a DEP field.

2 Results and Discussion

Monodisperse spherical particles of 3-(trimethoxysilyl)propyl methacrylate (TPM) were synthesized via spontaneous emulsification in the presence of F127 surfactant. Previous reports have demonstrated that under aqueous alkaline conditions, TPM monomers hydrolyze and subsequently condense into emulsion droplets, which then can be polymerized to form solid colloidal particles.³¹ Moreover, Cl groups can be introduced to the TPM particle surface by incorporating 3-chloro-2-hydroxypropyl methacrylate (CHPMA) during the polymerization step. Here, the Cl groups on the surface were transformed into amine (-NH_2) groups (Figure 2A). Gold was then deposited on the surface of the amine-functionalized TPM particles by reducing HAuCl_4 with NaBH_4 , which produced gold nuclei for subsequent growth of a smooth gold film upon treatment with a mixture of gold hydroxide and formaldehyde.³² The gold layer became smoother and more continuous with increasing NaBH_4 concentration in the first reduction step (Figure 2B-D). This can be attributed to larger numbers of gold nuclei that serve as growth centers, affording more evenly coated gold layers.

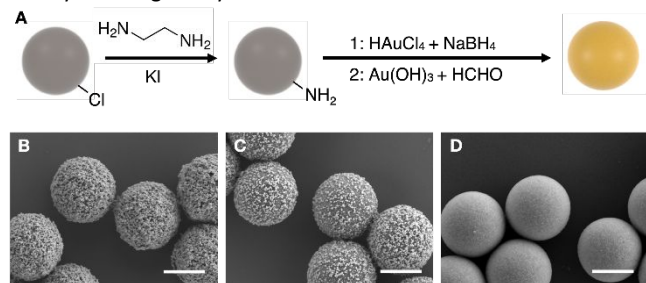


Fig. 2 (A) Synthesis of gold-coated TPM spheres. (B-D) SEM images of gold-coated TPM spheres treated with (B) 0.10 M, (C) 0.15 M, and (D) 0.50 M NaBH_4 , respectively. Scale bars = 1 μm .

Two- or three-lobed particles were fabricated using a protocol

illustrated in Figure 3, which is analogous to that previously reported by our laboratory that relied on controlled wetting of TPM monomer on TPM seed particles, with subsequent polymerization of the TPM monomer regions.¹⁵ Chlorine groups were introduced to the surface of either the seed or to new lobe(s) by combining CHPMA with TPM monomer prior to polymerization. Lobe-selective gold coating was then realized by converting the Cl groups to amines followed by gold reduction as described above.

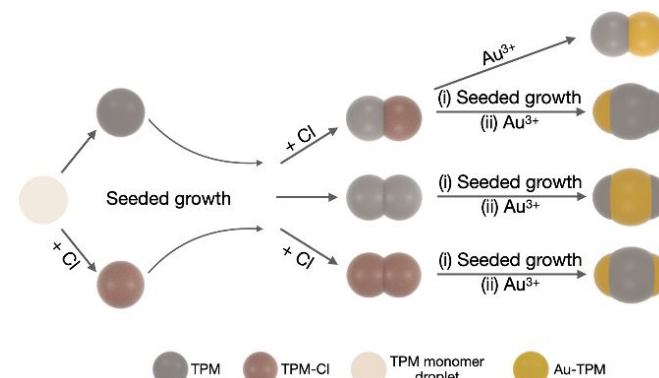


Fig. 3 Synthetic route for the fabrication of metalodielectric TPM particles.

Dumbbell-shaped **Au-T** dimers (T = TPM-only lobe) with chemically distinct lobes were prepared by addition of TPM monomer to Cl-functionalized TPM seeds, producing a dimer with only one lobe decorated with Cl (**2a**), followed by selective gold coating on the lobe corresponding to the initial seed using the amine protocol described above (Figure 4A). Scanning electron microscopy (SEM) revealed that each dimer had one lobe coated with gold (Figure 4B), which appears brighter in the SEM because gold is more conductive than TPM.¹⁸ Aqueous dispersions of these **Au-T** dimers are stable against aggregation (Figure 4C). Under an optical microscope, the gold-coated and uncoated lobes can be distinguished by their opaque and translucent appearance, respectively.

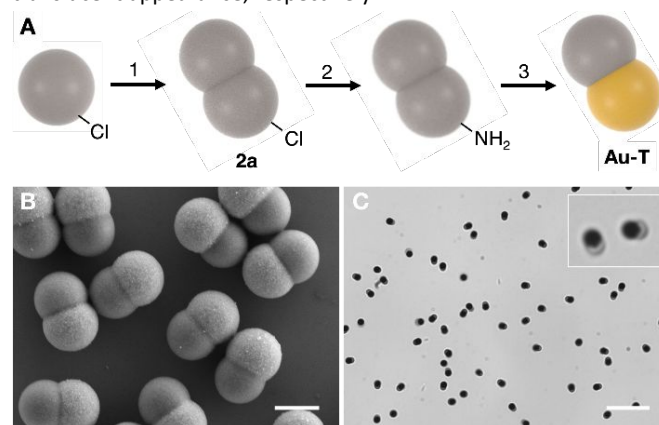


Fig. 4 (A) Synthesis of **Au-T** dimers. Step 1: Dimer **2a** fabrication via seeded growth polymerization; Step 2: Conversion of Cl groups to NH_2 groups; Step 3: Site-specific gold-coating. (B) SEM image of **Au-T** dimers. The brighter lobes correspond to those with gold coatings. (C) Optical micrograph of **Au-T** dimers. The gold lobes are opaque and the TPM lobes are translucent. Inset: Optical micrograph of two **Au-T** dimer particles. SEM image scale bar = 1 μm . Optical micrograph scale bar = 10 μm .

The three-lobed particle **3a** can be fabricated from dimer **2a** by the addition of TPM monomer to a fully polymerized dumbbell (Figure 5A, step 2). The TPM emulsion droplets wet the surfaces of both lobes of **2a**, eventually creating a belt-like lobe between the two lobes on the opposite ends.¹⁵ The size and shape of the central lobe was influenced by the surface wetting properties of **2a**, which can be regulated by the amount of F127 added during its fabrication (see Experimental Section). For example, a F127 concentration of 1.0 wt.% during the fabrication of **2a** resulted in a prominent belt-like lobe on **3a** (Figure 5A, step 2). Subsequent lobe-specific gold coating produced **Au-T-T** particles (Figure 5B, C).

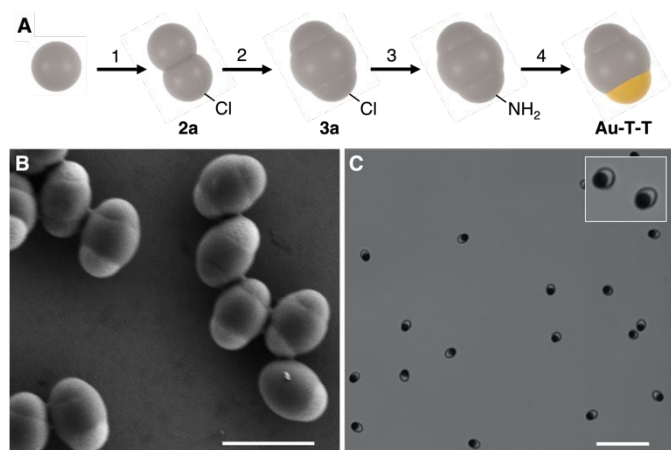


Fig. 5 (A) Synthesis of **Au-T-T** particles. Step 1: Fabrication of dimer **2a**; Step 2: Fabrication of three-lobe TPM particle **3a** via seeded growth polymerization on dimer **2a**, which creates a belt-like lobe around the center of the dimer; Step 3: Conversion of Cl groups to NH_2 groups; Step 4: Site-specific gold-coating. (B) SEM image and (C) optical micrograph of **Au-T-T** particles. Inset: Optical micrograph of two **Au-T-T** particles. SEM scale bar = 3 μm . Optical micrograph scale bar = 10 μm .

Au-T-Au particles can be fabricated from dimer **2b**, for which both lobes are decorated with Cl, enabling gold deposition on both ends (Figure 6).

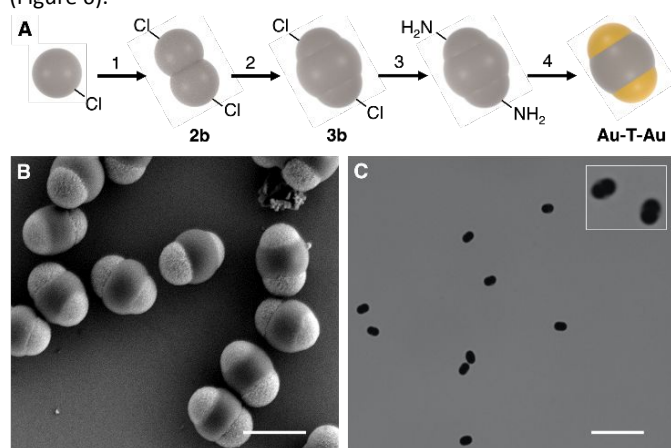


Fig. 6 (A) Synthesis of **Au-T-Au** particles. Step 1: Fabrication of dimer **2b**; Step 2: Fabrication of three-lobe TPM particle **3b** via seeded growth polymerization on dimer **2b**, which creates a belt-like lobe around the center of the dimer; Step 3: Conversion of Cl groups to NH_2 groups; Step 4: Site-specific gold-coating. (B) SEM image of linear **Au-T-Au** particles. (C) Optical

micrograph of **Au-T-Au** particles. Inset: Magnified optical micrograph of two particles. SEM scale bar = 2 μm . Optical micrograph scale bar = 10 μm .

T-Au-T particles can be fabricated by addition of TPM monomer and CHPMA to a suspension of particles **2c** in the presence of F127, followed by polymerization, which produced a central belt-like lobe with Cl groups for subsequent gold deposition. The size of the central lobe and its aspect ratio, w_c/h_c , can be adjusted by changing the concentration of TPM monomer (Figure 7).

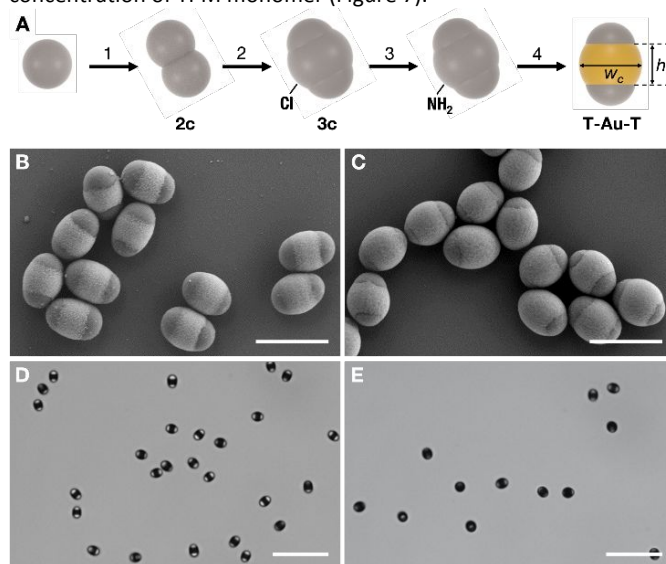


Fig. 7 (A) Synthesis of **T-Au-T** particles. Step 1: Fabrication of dimer **2c**; Step 2: Fabrication of three-lobe TPM particle **3c** in the presence of CHPMA via seeded growth polymerization on dimer **2c**, which creates a belt-like lobe around the center of the dimer; Step 3: Conversion of Cl groups to NH_2 groups; Step 4: Site-specific gold-coating. (B) SEM image and (D) optical micrograph of **T-Au-T** particles prepared with 0.2 wt% TPM; $w_c/h_c = 1.5$. (C) SEM image and (E) optical micrograph of **T-Au-T** particles prepared with 0.3 wt% TPM; $w_c/h_c = 1.1$. SEM scale bars = 3 μm . Optical micrograph scale bars = 10 μm .

2.1 Dielectrophoretic assembly of metallodielectric particles

Monodisperse particles were obtained using density gradient separation. Then the particles were dispersed in DI water and added to the channel of a DEP device that could be visualized with optical microscopy while applying an AC electric field (Figure S2). In a non-uniform electric field, a dielectrophoretic (DEP) force can either concentrate particles into a region of maximum field strength (positive DEP) or repel them from that region (negative DEP), depending on the relative dielectric constants of the particles and medium. The DEP force depends on E^2 , where E is the magnitude of the electric field, and the gradient of the field. In the presence of an electric field, particle assembly can be explained by a combination of dipolar interparticle interactions.²¹

Under an AC electric field of 200 V/cm at a frequency of 10 kHz the **Au-T** dimers aligned normal to the x - y plane with the gold lobes resting on the lower surface of the DEP cell where the electric field is concentrated in the x - y plane between the two opposing 40 nm-thick electrodes (Figure S2). The preference for this orientation is not unexpected given the higher dielectric constant and polarizability of the gold-coated lobes compared with the TPM lobes, resulting in

more favorable interactions between the electric field and the induced dipoles in gold end of the particle.^{18, 21, 28, 33} These **Au-T** particles organized into chains with interparticle TPM-TPM and Au-Au contacts with retention of the particle orientation (Figure 8A). These observations suggest that formation of the chain-like structures is dominated by the induced dipoles on the gold lobes located at the lower surface. Whereas a frequency of 1 kHz did not provoke chain assembly (Figure 8B), chains comprising as many as six **Au-T** dimers were observed at 10 kHz (Figure 8C) and longer chains were observed at 100 kHz (Figure 8D). Analysis of randomly selected images revealed that approximately 73% of the chains formed at 10 kHz ranged from one to four dimers (Figure 8E), whereas 75% of the chains at 100 kHz contained five or more dimers (see Supporting Information). The frequency-dependent chain formation was reversible (Video S1).

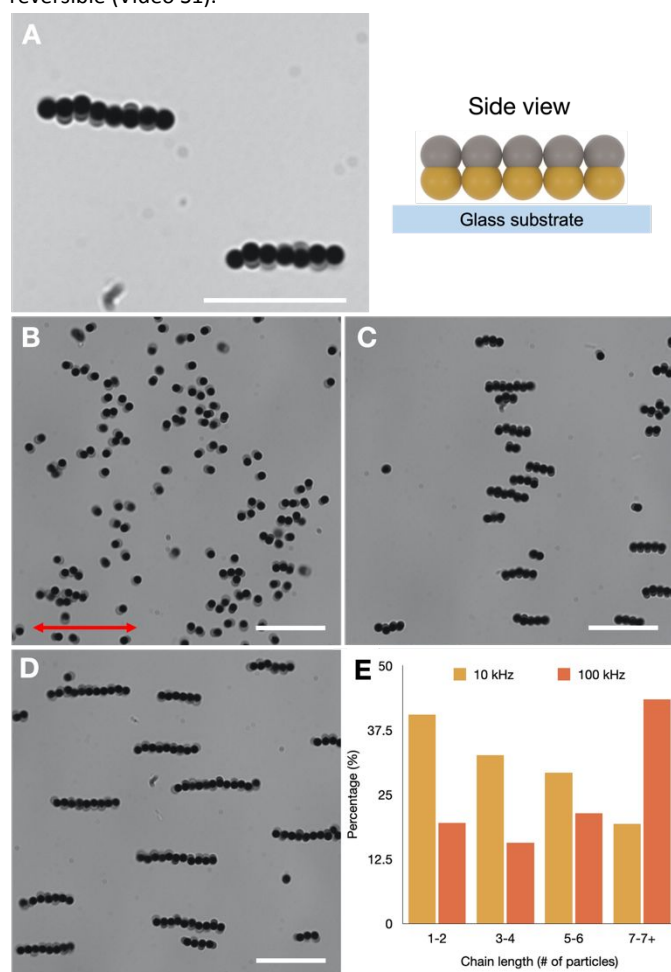


Fig. 8 (A) Optical micrograph of chains of **Au-T** dimers. The schematic on the right illustrates the side view of the chain structure. (B-D) Optical micrographs of **Au-T** chains after applying an electric field for 10 minutes at (B) 1 kHz, (C) 10 kHz, and (D) 100 kHz, respectively. (E) Histogram of the percentage of chains at various chain lengths at 200 V/cm and 10 and 100 kHz. Scale bars = 10 μm .

The response of **Au-T-T** particles to the DEP field was similar to that of the **Au-T** particles. At a field strength of 200 V/cm at 10 kHz, the gold-coated lobe of each **Au-T-T** particle rested on the lower surface of the DEP cell where the electric field is

concentrated, with the long axis of each particle oriented along the z-axis. The **Au-T-T** particles slowly formed chain structures with contacts between the large waist of the middle lobes (Figure 9A). These chains also appear to be less uniform than the **Au-T** chains with respect to interparticle contacts. The chains gradually transform into a disordered ensemble over approximately one hour under the AC field (Figure 9B). The different behaviors observed for **Au-T** and **Au-T-T** can be attributed to differences in the local non-uniform electric fields induced around the particles.³⁴ The dielectric constant of the gold lobe is larger than that of the surrounding media, which favors concentration of the particles, via the gold lobes, in regions of maximum field strength (positive DEP).^{21, 30}

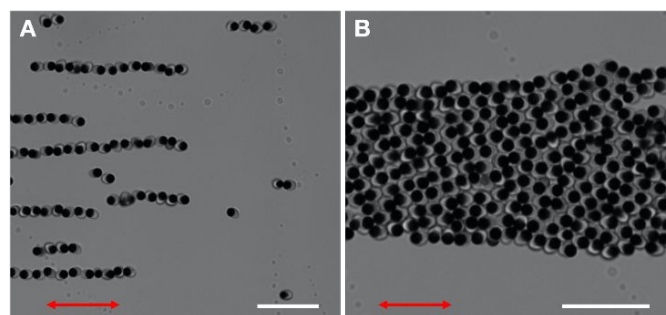


Fig. 9 Optical micrographs of **Au-T-T** (A) chains and (B) 2D aggregates in an electric field (200 V/cm, 10 kHz). Optical micrograph scale bars = 10 μm .

The local electric field intensity distributions for chains of three particles, calculated with COMSOL at the central planes of the gold lobes (green plane) and TPM lobes (gray plane), reveal that the maximum field strength exists at the ends of the **Au-T** chains, with minima along the center of the chain. Consequently, the positive-DEP gold lobes would be attracted to the ends of the chains, favoring chain growth, but aggregation of **Au-T** chains into 2D ensembles would be disfavored as this would require unfavorable approach of the gold lobes to regions of minimum electric field (Figure 10). The central TPM lobes of the **Au-T-T** particles bulge from the center, introducing a steric hindrance that can reduce dipolar interactions between the gold lobes and may account for the disorder within the **Au-T-T** chains. COMSOL modeling of the electric field at the central plane of the TPM lobes in the **Au-T-T** particles suggests that chain aggregation would allow nesting of TPM lobes on adjacent chains in regions of field minima, which is essential to the formation of an ordered 2D ensemble. Interchain nesting, however, would require the positive-DEP gold lobes to be located in regions of minimum electric field, which would frustrate interchain ordering, as observed in Figure 9B.

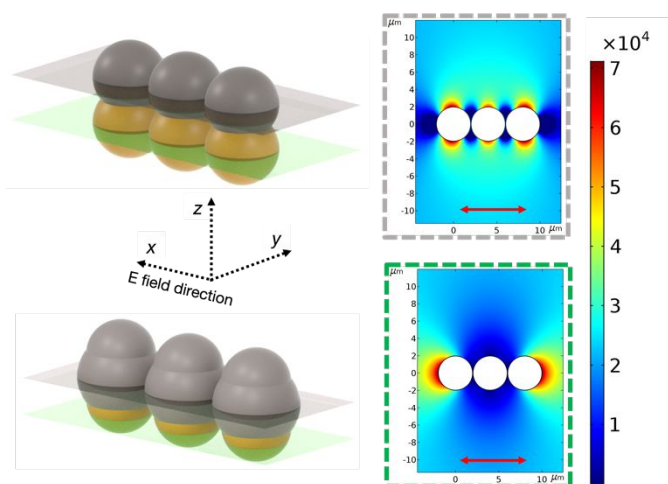


Fig. 10 COMSOL simulations of the local electric field intensity distribution around particles in a chain. The electric field intensity distribution in the gray and green boxes correspond to the planes defined by the centers of the TPM and Au lobes, respectively. Red arrows indicate the direction of the electric field. Color bar indicates the electric field strength.

Under the influence of the DEP field, T-Au-T particles lay “flat” such that their long axes are parallel to the x-y plane of the DEP cell. Moreover, alignment of the particles in the x-y plane depends on the aspect ratio of the central gold lobe, with their long axes either perpendicular (Figure 11A, $w_c/h_c = 1.5$) or parallel (Figure 11B, $w_c/h_c = 1.1$) to the field direction. In the case of T-Au-T particles with $w_c/h_c = 1.5$, the induced dipole moment is expected to be larger along the w_c direction than along h_c , consistent with the observed particle alignment. When $w_c/h_c = 1.1$, however, w_c is comparable with h_c , and the dipoles induced in the two TPM lobes can exert a relatively greater influence such that the particles align along the w_c/h_c direction.

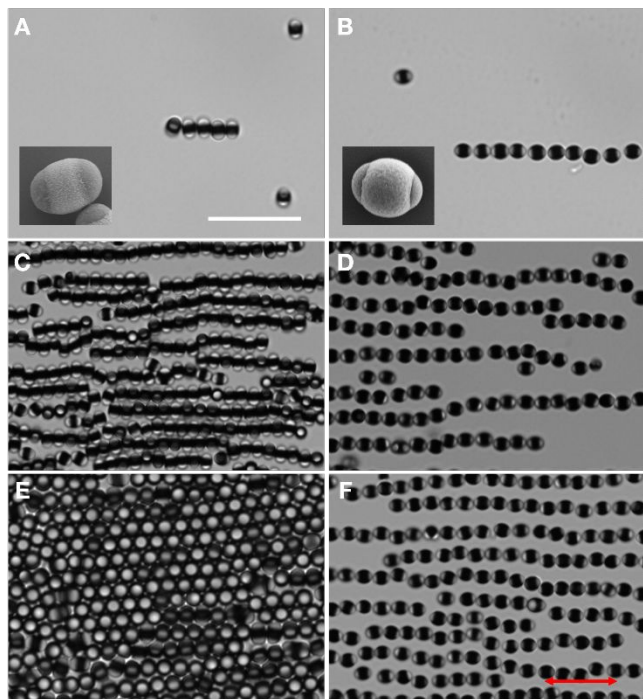


Fig. 11 (A, B) Optical micrographs of T-Au-T ($w_c/h_c = 1.5$) and T-Au-T ($w_c/h_c = 1.1$) particles at low concentrations (0.1% wt), respectively. The corresponding SEM images are provided in the insets. (C,D) T-Au-T ($w_c/h_c = 1.5$) and T-Au-T ($w_c/h_c = 1.1$) particles at high concentrations (1.0% wt) ten minutes after application of the electric field. (E,F) T-Au-T ($w_c/h_c = 1.5$) and T-Au-T ($w_c/h_c = 1.1$) particles, respectively, at 1.0% wt two hours after application of the electric field. The higher concentration (1.0% wt) selected for the particles’ assembly is the same in C-F, and this concentration is sufficient for particles to form 2D assemblies. Scale bar in panel A is 10 μm , and it is the same for all optical micrographs. The red arrow in panel F indicates the direction of the electric field for all DEP cell images.

Both $w_c/h_c = 1.5$ and 1.1 particles gradually grew into chain structures along the field direction (Figure 11C, D, Figure S4). The particles in chains of T-Au-T ($w_c/h_c = 1.5$) retained their alignment with respect to the x-y plane and the electric field. Surprisingly, they eventually assembled into hexagonal 2D domains under the applied field accompanied by a 90° “flip” of the particles such that their long axes were now aligned with the z-direction rather than in the x-y plane (Figure 11E). The hexagonal packing is likely favored by the nearly cylindrical shape of the $w_c/h_c = 1.5$ particles combined with favorable dipolar interactions between the TPM lobes now in contact with the lower surface of the DEP cell where the electric field is strongest. This configuration also may be preferred over a 2D ensemble with the particles perpendicular to the z-direction that would require negative-DEP TPM lobes and positive-DEP Au lobes to be co-located in the x-y plane.

Chains of T-Au-T ($w_c/h_c = 1.1$) did not form 2D lattices, however, remaining separate even after two hours (Figure 11F). This may be attributed to repulsive Au-Au and TPM-TPM dipole-dipole forces between in non-staggered chains or repulsive Au-TPM forces in staggered chains where the Au-lobes would be nested in the TPM regions of an adjacent chain (Figure S5). The absence of a 2D ensemble with the particles flipped 90° may be attributed to a “dipole trap” in which there exists an inherent barrier to particle rotation against the electric field direction. Such a barrier does not exist for the $w_c/h_c = 1.5$ particles because the particles are aligned in a manner that they flip about the electric field direction. Moreover, if the barrier for the $w_c/h_c = 1.1$ particles was surmounted, their shape would likely introduce a packing frustration that would not allow for interparticle contact along their entire surface because of the more oblate shape.²⁸

Conclusions

This contribution introduces a new synthetic methodology for the fabrication of metallodielectric multi-component particles with shape and compositional surface anisotropy. Selective incorporation of $-\text{NH}_2$ groups on the surfaces of particle lobes enabled the formation of anisotropic dumbbells with one lobe coated with gold (Au-T) as well as the formation of three distinct trimers Au-T-T, Au-T-Au, and T-Au-T. Under DEP fields, the Au-T particles aligned vertically and formed chains as a consequence of the highly polarized gold lobe, with chain lengths increasing with increasing field frequency.

Au-T-T particles assembled into chains, similar to the assembly of the **Au-T** particles, but they gradually formed disordered 2D aggregates. Interestingly, the assembly of **T-Au-T** was influenced by the aspect ratio of the gold-coated central lobe, aligning orthogonal or parallel to the field direction for higher and lower aspect ratios, respectively, the former coalescing into 2D lattices. These observations provide further evidence for the utility of synthetic design and regioselective modification of patchy particles for regulating the assembly of 2D materials on the colloidal length scale.

Conflicts of interest

There are no conflicts to declare.

Acknowledgements

This work was supported by the Department of Energy under Grant Award No. DE-SC0007991. The authors acknowledge the use of shared facilities provided through the Materials Research Science and Engineering Center (MRSEC) program of the National Science Foundation under Award Number DMR-1420072. V.G. acknowledges support from the Margaret Strauss Kramer Fellowship.

References

1. Y. Xia, B. Gates, Y. Yin and Y. Lu, *Adv. Mater.*, 2000, **12**, 693-713.
2. S. Sacanna and D. J. Pine, *Curr. Opin. Colloid Interf. Sci.*, 2011, **16**, 96-105.
3. S. C. Glotzer and M. J. Solomon, *Nat. Mater.*, 2007, **6**, 557-562.
4. Y. Wang, Y. Wang, D. R. Breed, V. N. Manoharan, L. Feng, A. D. Hollingsworth, M. Weck and D. J. Pine, *Nature*, 2012, **491**, 51-55.
5. Q. Chen, S. C. Bae and S. Granick, *Nature*, 2011, **469**, 381-384.
6. M. Liu, X. Zheng, V. Grebe, D. J. Pine and M. Weck, *Nat. Mater.*, 2020, **19**, 1354-1361.
7. M. He, J. P. Gales, É. Ducrot, Z. Gong, G. R. Yi, S. Sacanna and D. J. Pine, *Nature*, 2020, **585**, 524-529.
8. S. C. Glotzer, *Nature*, 2012, **481**, 450-452.
9. K. J. Stebe, E. Lewandowski and M. Ghosh, *Science*, 2009, **325**, 159-160.
10. T. Wink, S. J. van Zuilen, A. Bult and W. P. van Bennekom, *Analyst*, 1997, **122**, 43R-50R.
11. S. Coyle, G. V. Prakash, J. J. Baumberg, M. Abdelsalem and P. N. Bartlett, *Appl. Phys. Lett.*, 2003, **83**, 767-769.
12. B. Bharti and O. D. Velev, *Langmuir*, 2015, **31**, 7897-7908.
13. P. Song, B. K. Olmsted, P. Chaikin and M. D. Ward, *Langmuir*, 2013, **29**, 13686-13693.
14. B. J. Park and E. M. Furst, *Langmuir*, 2010, **26**, 10406-10410.
15. M. Liu, F. Dong, N. S. Jackson, M. D. Ward and M. Weck, *J. Am. Chem. Soc.*, 2020, **142**, 16528-16532.
16. O. Cayre, V. N. Paunov and O. D. Velev, *J. Mater. Chem.*, 2003, **13**, 2445-2450.
17. Y. Wang, Y. Wang, X. Zheng, É. Ducrot, M.-G. Lee, G.-R. Yi, M. Weck and D. J. Pine, *J. Am. Chem. Soc.* 2015, **137**, 10760-10766.
18. S. Gangwal, O. J. Cayre and O. D. Velev, *Langmuir*, 2008, **24**, 13312-13320.
19. B. Bharti, F. Kogler, C. K. Hall, S. H. L. Klapp and O. D. Velev, *Soft Matter*, 2016, **12**, 7747-7758.
20. O. D. Velev and K. H. Bhatt, *Soft Matter*, 2006, **2**, 738-750.
21. O. D. Velev, S. Gangwal and D. N. Petsev, *Annu. Rep. Prog. Chem., Sect. C: Phys. Chem.* 2009, **105**, 213-246.
22. M. Trau, D. A. Saville and I. A. Aksay, *Science*, 1996, **272**, 706-709.
23. D. C. Prieve, P. J. Sides and C. L. Wirth, *Curr. Opin. Colloid Interf. Sci.*, 2010, **15**, 160-174.
24. M. T. Sullivan, K. Zhao, A. D. Hollingsworth, R. H. Austin, W. B. Russel and P. M. Chaikin, *Phys. Rev. Lett.*, 2006, **96**, 015703.
25. P. Song, Y. Wang, Y. Wang, A. D. Hollingsworth, M. Weck, D. J. Pine and M. D. Ward, *J. Am. Chem. Soc.*, 2015, **137**, 3069-3075.
26. Z. Jia, J. H. Kim, G. R. Yi and S. S. Lee, *Langmuir*, 2018, **34**, 12412-12418.
27. N. Yanai, M. Sindoro, J. Yan and S. Granick, *J. Am. Chem. Soc.*, 2013, **135**, 34-37.
28. Z. Wang, Z. Wang, J. Li and Y. Wang, *ACS Nano*, 2021, **15**, 5439-5448.
29. S. Gangwal, A. Pawar, I. Kretzschmar and O. D. Velev, *Soft Matter*, 2010, **6**, 1413-1418.
30. F. Dong, M. Liu, V. Grebe, M. D. Ward and M. Weck, *Chem. Mater.*, 2020, **32**, 6898-6905.
31. C. van der Wel, R. K. Bhan, R. W. Verweij, H. C. Frijters, Z. Gong, A. D. Hollingsworth, S. Sacanna and D. J. Kraft, *Langmuir*, 2017, **33**, 8174-8180.
32. T. Sainsbury, T. Ikuno, D. Okawa, D. Pacilé, J. M. J. Fréchet and A. Zettl, *J. Phys. Chem. C*, 2007, **111**, 12992-12999.
33. T. Jones, *Press, Cambridge*, 1995.
34. Y. Alapan, B. Yigit, O. Beker, A. F. Demirörs and M. Sitti, *Nat. Mater.*, 2019, **18**, 1244-1251.